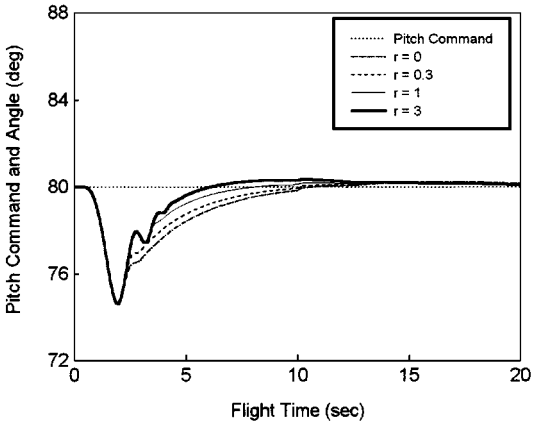

Fig. 3 Simulation results by modified AWC with $b = 1.0$.

in the control parameters. With this in mind, the preceding AWC is modified so that the modified AWC protects the integrator from being a large negative value in the initial control phase by limiting the PD terms of the compensator output for the AW feedback. In other words, if we let δ_{p1} and δ_{p2} represent the PD and integral terms of the compensator output, respectively, the controller takes the saturated values of δ_{p1} and δ_{p2} as the AW feedback signal. The modified AWC approach is constructed as

$$f = (1/T_t)\left[\min(\delta_{p1}, H) - u_p^w + \delta_{p2}\right] \tag{9}$$

where H is the saturated value of δ_{p1}, which limits the combination of proportional and derivative terms of the compensator output. A ratio of the saturated value of the actuator to H determines the modification quantities in the modified AWC

$$r = H_{\text{act}}/H \tag{10}$$

where H_{act} is the saturated values of the actuator, which is 22 deg for S-19. The attitude control performance of this modified AWC is presented in Fig. 3. It represents a case when the modified AWC is applied to the typical AWC with a large value of AW gain b. This case also corresponds to the slow response, as was discussed earlier. Note that the response characteristic has improved significantly. The change in the control system performance is not very large considering the same range of variation of r as in the AW gain of Fig. 1. These results prove the desirable performance of the modified AWC for the case of slow dynamic responses. It also shows that the modified AWC is not that sensitive to changes of the control parameter r. On the other hand, as the parameter r increases, the stability margin of the control system reduces gradually. However, closed-loop stability is guaranteed with the modified AWC if the original PID controller is stable.

Conclusions

Design of a typical and a modified AWC in the presence of actuator saturation of KSR-II is investigated. The control performance of the typical AWC turned out to be rather sensitive to the AW gain with slower response characteristics for a large AW gain. This has been partially resolved by introducing a modified AWC. The modified AWC improved the slow response considerably, even with a large AW gain. This modified AWC showed less sensitivity to the control gains compared with the typical AWC.

References

[1]Ljunge, L., and Hall, L., "S19 Guidance of the Black Brant X Sounding Rocket," *Journal of Guidance, Control, and Dynamics*, Vol. 7, No. 2, 1984, pp. 156–160.

[2]Hanus, R., Kinnaert, M., and Henrotte, J. L., "Conditioning Technique, a General Anti-Windup and Bumpless Transfer Method," *Automatica*, Vol. 23, No. 6, 1987, pp. 729–739.

[3]Kothare, M. V., Campo, P. J., Morari, M., and Nett, C. N., "A Unified Framework for the Study of Anti-Windup Designs," *Automatica*, Vol. 30, No. 12, 1994, pp. 1869–1883.

[4]Megretski, A., and Rantzer, A., "System Analysis via Integral Quadratic Constraints," *IEEE Transactions on Automatic Control*, Vol. 42, No. 6, 1997, pp. 819–830.

[5]Kothare, M. V., and Morari, M., "Multiplier Theory for Stability Analysis of Anti-Windup Control Systems," *Proceedings of the 34th Conference on Decision and Control* (New Orleans, LA), 1995, pp. 3767–3772.

[6]Nagraph, I. J., and Gopal, M., *Control Systems Engineering*, Wiley, New Delhi, India, 1982, pp. 625–642.

Artificial Lagrange Points for a Partially Reflecting Flat Solar Sail

Colin R. McInnes*
University of Glasgow, Glasgow, Scotland G12 8QQ, United Kingdom

I. Introduction

PREVIOUS studies have demonstrated that families of artificial Lagrange points may be generated using solar sail spacecraft.[1,2] However, these studies assumed an idealized solar sail with perfect reflectivity. This Note will reexamine the problem with a partially reflecting solar sail because a real aluminized sail film would typically have a reflectivity on the order of 0.9. First, equilibrium solutions will be obtained for an ideal flat solar sail. Then the problem will be revisited with a partially reflecting solar sail. Apart from reducing the magnitude of the radiation pressure force exerted on the solar sail, the finite absorption of the sail means that the radiation pressure force vector is no longer directed normal to the sail surface. Because of this effect, it will be shown that the volume of space available for artificial Lagrange points is extremely sensitive to the solar sail reflectivity. These artificial Lagrange points are of interest for a number of mission applications.[3–5]

II. Equilibrium Solutions for an Ideal Flat Solar Sail

First equilibrium solutions for an idealized, perfectly reflecting flat solar sail will be generated. We will not consider compound solar sails such as the solar photon thruster concept of Forward.[6] The ideal sail will be considered in a frame of reference corotating with two primary masses m_1 (Sun) and m_2 (Earth or another planet) at constant angular velocity $\boldsymbol{\omega}$, as shown in Fig. 1. The sail attitude is defined by a unit vector $\boldsymbol{n}$ normal to the sail surface, fixed in the rotating frame of reference. In addition, the ratio of the solar radiation pressure force to the solar gravitational force exerted on the sail is defined by the sail lightness number β. Because both forces have an inverse square variation with solar distance, the sail lightness number is a constant. It can be shown that the sail lightness number is related to the total solar sail mass per unit area by $\sigma\,(\mathrm{g\,m^{-2}}) = 1.53/\beta$. The units of the problem will be chosen such that the gravitational constant, the distance between the two primary masses, and the sum of the primary masses are all taken to be unity.

The vector equation of motion for a solar sail in this rotating frame of reference may be written in standard form as

$$\frac{\mathrm{d}^2\boldsymbol{r}}{\mathrm{d}t^2} + 2\boldsymbol{\omega} \times \frac{\mathrm{d}\boldsymbol{r}}{\mathrm{d}t} + \nabla U = \boldsymbol{a} \tag{1}$$

where the three-body gravitational potential U and the solar radiation pressure acceleration $\boldsymbol{a}$ are defined by

$$U = -\left\{\tfrac{1}{2}(x^2 + y^2) + [(1-\mu)/r_1] + (\mu/r_2)\right\} \tag{2a}$$

$$\boldsymbol{a} = \beta\left[(1-\mu)/r_1^2\right](\hat{\boldsymbol{r}}_1 \cdot \boldsymbol{n})^2\boldsymbol{n} \tag{2b}$$

Received June 12, 1998; revision received Aug. 17, 1998; accepted for publication Sept. 7, 1998.

*Reader, Department of Aerospace Engineering. E-mail: colinmc@aero.gla.ac.uk.

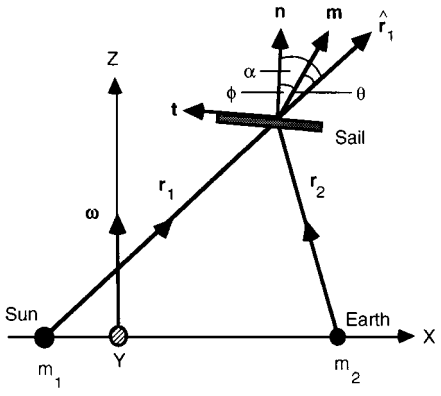

Fig. 1 Sun–Earth restricted three-body problem with a partially reflecting solar sail.

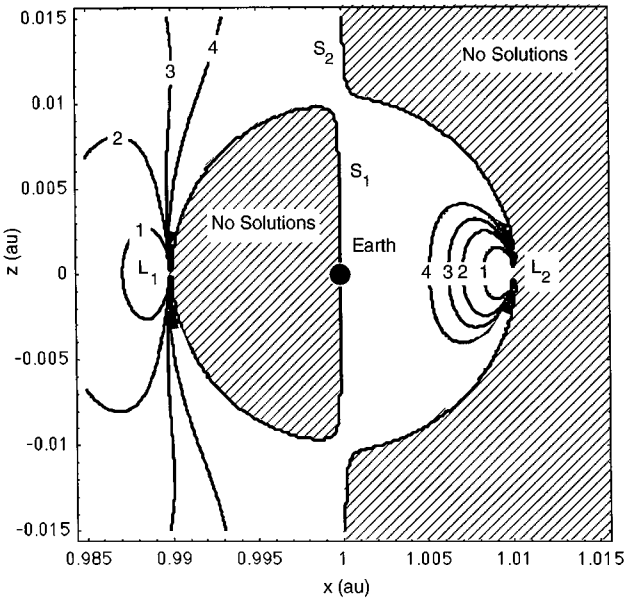

Fig. 2 Contours of sail lightness numbers in the x–z plane with $\eta = 1$. Contours: 1—0.02, 2—0.04, 3—0.06, and 4—0.1.

where $\mu = m_2/(m_1 + m_2)$ is the mass ratio of the system and the sail position vectors are defined as $\boldsymbol{r}_1 = (x + \mu, y, z)$ and $\boldsymbol{r}_2 = [x - (1 - \mu), y, z]$.

Equilibrium solutions are now required in the rotating frame of reference so that the first two terms of Eq. (1) vanish. The five classical Lagrange points are then defined as the solutions to $\nabla U = 0$ with $\hat{\boldsymbol{r}}_1 \cdot \boldsymbol{n} = 0$, and so $\boldsymbol{a} = 0$. However, for $\hat{\boldsymbol{r}}_1 \cdot \boldsymbol{n} \succ 0$ there is an additional acceleration $\boldsymbol{a}$ that is a function of the lightness number β and attitude $\boldsymbol{n}$ so that new artificial equilibrium solutions may be generated. Because the vector $\boldsymbol{a}$ is oriented in direction $\boldsymbol{n}$, taking the vector product of $\boldsymbol{n}$ with Eq. (1) it follows that

$$\nabla U \times \boldsymbol{n} = 0 \Rightarrow \boldsymbol{n} = \lambda \nabla U \tag{3}$$

where λ is an arbitrary scalar multiplier. Using the normalization condition $|\boldsymbol{n}| = 1$, λ is identified $|\nabla U|^{-1}$ so that the required sail attitude is defined by

$$\boldsymbol{n} = \nabla U / |\nabla U| \tag{4}$$

The required sail lightness number may also be obtained by taking a scalar product of Eq. (1) with $\boldsymbol{n}$. Again requiring an equilibrium solution it is found that

$$\beta = \frac{r_1^2}{(1 - \mu)} \frac{\nabla U \cdot \boldsymbol{n}}{(\hat{\boldsymbol{r}}_1 \cdot \boldsymbol{n})^2} \tag{5}$$

Because the sail lightness number and attitude can in principle be freely chosen, the set of five classical Lagrange points will be replaced by an infinite set of artificially generated equilibrium solutions.

The regions in which these new solutions may exist are defined by the constraint $\hat{\boldsymbol{r}}_1 \cdot \nabla U \geq 0$ with a boundary surface defined by an equality. This constraint may be understood physically because the solar radiation pressure acceleration vector $\boldsymbol{a}$, and so the sail attitude vector $\boldsymbol{n}$, can never be directed sunward. The boundary surface has two topologically disconnected surfaces S_1 and S_2 that define the region of existence of equilibrium solutions near m_2, as shown in Fig. 2. The classical equilibrium solutions lie on either S_1 or S_2 because they are the solutions to $\nabla U = 0$. In general, the surfaces of constant sail lightness number approach these boundaries asymptotically with $\beta \to \infty$ when $\hat{\boldsymbol{r}}_1 \cdot \nabla U \to 0$ as is clear from Eq. (5). Surfaces of constant sail lightness number generated from Eq. (5) for the Earth–Sun system are shown in Fig. 2. It can be seen that as the sail lightness number increases larger volumes of space are accessible for artificial equilibrium points.

III. Equilibrium Solutions for a Partially Reflecting Flat Solar Sail

A realistic flat solar sail force model that includes absorption will now be considered. To allow a closed-form solution, the solar sail will be assumed to have perfect specular reflectivity and no thermal reemission but will still have an overall reflectivity η less than unity. Then the radiation pressure acceleration will act in direction $\boldsymbol{m}$ and may be written as the sum of components normal $\boldsymbol{n}$ and transverse $\boldsymbol{t}$ to the sail surface[7]:

$$a\boldsymbol{m} = \tfrac{1}{2}\beta\left(\mu / r_1^2\right)(1 + \eta)(\hat{\boldsymbol{r}}_1 \cdot \boldsymbol{n})^2 \boldsymbol{n} + \tfrac{1}{2}\beta\left(\mu / r_1^2\right)(1 - \eta)(\hat{\boldsymbol{r}}_1 \cdot \boldsymbol{n})(\hat{\boldsymbol{r}}_1 \cdot \boldsymbol{t})\boldsymbol{t} \tag{6}$$

It can be seen that the main effect of the nonperfect reflectivity of the sail is to reduce the acceleration magnitude and to introduce an offset in the direction of the radiation pressure acceleration. The acceleration now acts in direction $\boldsymbol{m}$ rather than normal to the sail surface in direction $\boldsymbol{n}$. This offset is defined by the centerline angle ϕ with the actual radiation pressure force direction defined by the cone angle θ, as shown in Fig. 1.

The analysis presented in the previous section will be repeated using the sail force model defined by Eq. (6) so that the equation of motion may now be written as

$$\frac{\mathrm{d}^2 \boldsymbol{r}}{\mathrm{d}t^2} + 2\boldsymbol{\omega} \times \frac{\mathrm{d}\boldsymbol{r}}{\mathrm{d}t} + \nabla U = a\boldsymbol{m} \tag{7}$$

For an equilibrium solution the first two terms of Eq. (7) will again vanish so that the sail attitude must be chosen as

$$\boldsymbol{m} = \nabla U / |\nabla U| \tag{8}$$

The unit vector $\boldsymbol{m}$ can now be defined by the cone angle θ between the radial direction $\hat{\boldsymbol{r}}_1$ and $\boldsymbol{m}$ as

$$\tan\theta = \frac{|\hat{\boldsymbol{r}}_1 \times \nabla U|}{\hat{\boldsymbol{r}}_1 \cdot \nabla U} \tag{9}$$

In addition, using Eq. (6) the centerline angle can be obtained from the ratio of the transverse and normal accelerations as

$$\tan\phi = [(1 - \eta)/(1 + \eta)] \tan\alpha \tag{10}$$

Noting that $\boldsymbol{n} \cdot \boldsymbol{t} = 0$ and taking a scalar product of Eq. (7) with the unit vector $\boldsymbol{n}$ gives the required sail lightness number as

$$\beta = \frac{2r_1^2}{\mu} \frac{\nabla U \cdot \boldsymbol{n}}{(1 + \eta)(\hat{\boldsymbol{r}}_1 \cdot \boldsymbol{n})^2} \tag{11}$$

The centerline angle may be obtained explicitly by noting that $\alpha = \theta + \phi$. Then, after some reduction, Eq. (10) yields the centerline angle directly from the cone angle as[7]

$$\tan\phi = \frac{\eta}{(1 + \eta)\tan\theta}\left[1 - \left(1 - \frac{1 - \eta^2}{\eta^2}\tan^2\theta\right)^{\frac{1}{2}}\right] \tag{12}$$

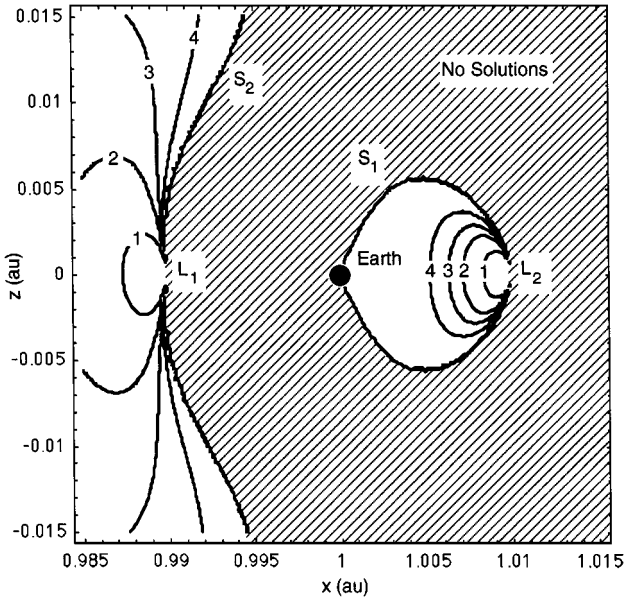

Fig. 3 Contours of sail lightness numbers in the x–z plane with $\eta = 0.9$. Contours: 1—0.02, 2—0.04, 3—0.06, and 4—0.1.

Lastly, using Eq. (11), it is found that the required sail lightness number may be obtained in terms of the lightness number for an ideal solar sail $\tilde{\beta}$ as

$$\beta = \frac{2}{(1+\eta)} \frac{\sqrt{1+\tan^2\phi}}{(1-\tan\theta\tan\phi)^2} \tilde{\beta} \tag{13}$$

where $\tilde{\beta}$ is defined by Eq. (5). Therefore, using Eqs. (9), (12), and (13), one can obtain the sail orientation and lightness number required for an equilibrium solution.

The effect of a nonideal flat solar sail is shown in Fig. 3 for a reflectivity of 0.9, typical of an aluminized sail film. First it can be seen that the volume of space available for equilibrium solutions about L_2 is significantly reduced. This is due to the centerline angle, which limits the direction in which the radiation pressure force vector can be oriented. For solutions near L_1 the main effect of the nonideal sail is to displace the equilibrium solutions toward Earth. This is due to the reduction in the magnitude of the radiation pressure force rather than the centerline angle.

IV. Conclusions

It has been shown that a partially reflecting solar sail can be used to generate artificial Lagrange points in Sun–planet three-body systems. However, the nonperfect reflectivity of the solar sail can have a significant effect on the volume of space in which such equilibrium solutions are possible. The main reason for the sensitivity of the problem to the sail reflectivity is the centerline angle, which limits the direction in which the radiation pressure force vector can be oriented.

References

[1]McInnes, C. R., and MacPherson, K. P., "Solar Sail Halo Trajectories: Dynamics and Applications," 42nd International Astronautical Congress, IAF Paper 91-334, Oct. 1991.

[2]McInnes, C. R., McDonald, A. J. C., Simmons, J. F. L., and MacDonald, E. W., "Solar Sail Parking in Restricted Three-Body Systems," *Journal of Guidance, Control, and Dynamics*, Vol. 17, No. 2, 1994, pp. 399–406.

[3]Forward, R. L., "Statite: A Spacecraft That Does Not Orbit," *Journal of Spacecraft and Rockets*, Vol. 28, No. 5, 1991, pp. 606–611.

[4]Carroll, K. A., "POLARES Solar Sail Feasibility Study Results—Part 1," Dynacon Ltd., Dynacon TM 39-306/04-1, Downsview, ON, Canada, Oct. 1993.

[5]West, J. L., "NOAA/DoD/NASA Geostorm Warning Mission," Jet Propulsion Lab., JPL D-13986, Pasadena, CA, Oct. 1996.

[6]Forward, R. L., "Solar Photon Thrustor," *Journal of Spacecraft and Rockets*, Vol. 27, No. 4, 1990, pp. 411–416.

[7]Molostov, A. A., and Shvartsburg, A. A., "Heliocentric Halos for a Solar Sail with Absorption," *Soviet Physics Doklady*, Vol. 37, No. 3, 1992, pp. 149–152.

Simple Correction Algorithm of Scanning Horizon Sensor Measurement for Earth Oblateness

Jie Li*
Stanford University, Stanford, California 94305-4085

Introduction

THE scanning horizon sensor is widely utilized in the Earth-pointing satellite to estimate its attitude with respect to the local vertical, i.e., roll and pitch angles. It typically uses an infrared detector together with a pencil beam to sense the abrupt change in the infrared radiation intensity as the beam sweeps from cold space across the horizon. The beam scans the horizon either by using an internal mechanism (such as an oscillating mirror, a motor-driven rotating reflective or refractive optic, etc.) or by mounting the sensor on a bias momentum wheel. Although the scan mechanisms are different, the operating principle of the scanning horizon sensors can be generally described as follows: The field of view (FOV) of the infrared detector diverts from the spin axis at a specific angle and traces out a cone (or part of a cone) as the sensor scans. The rising pulse and the falling pulse are generated as the Earth's horizon is encountered going from cold space, across the Earth, and then back into cold space. Given the fixed sensor reference, the phase angles of the horizon crossing points, which define the geometric intersection of the scan cone with the Earth, can be measured from the timing of the pulses, and the roll and pitch angles of the satellite are estimated. Because the Earth is not an exact sphere, but approximately an oblate spheroid relative to the polar axis, the Earth oblateness must be corrected in the attitude estimation, or an attitude error will remain. Several authors (e.g., Ref. 1 and the references therein) have studied the impact of the Earth oblateness on the attitude errors, but most of results have been scattered in the open literature and internal technical documents.

In this Note a simple algorithm is presented to correct the scanning horizon sensor measurement for the Earth oblateness in the satellite attitude estimation. Compared with the method described in Ref. 2, the problem is transferred from solving a three-dimensional vector equation of the horizon crossing vector to solving a scalar equation of the phase angle of the horizon crossing point, and the algorithm is simplified. Considering that the flattening coefficient of the oblate Earth is small, a first-order correction algorithm is also derived, which achieves relatively high accuracy with much simpler computation.

Reference Frames

Define several reference frames as follow: 1) the geocentric-equatorial inertial frame $O_I - \boldsymbol{X}_I\boldsymbol{Y}_I\boldsymbol{Z}_I$, where O_I is the center of the Earth, $\boldsymbol{X}_I$ points in the vernal equinox direction, $\boldsymbol{Z}_I$ points to the North Pole, and $\boldsymbol{Y}_I$ completes the right-handed triad; 2) the satellite body frame $O_B - \boldsymbol{X}_B\boldsymbol{Y}_B\boldsymbol{Z}_B$, where O_B is the mass center of the satellite, and $\boldsymbol{X}_B$, $\boldsymbol{Y}_B$, and $\boldsymbol{Z}_B$ are the body-fixed roll, pitch, and yaw axes, respectively; 3) the horizon sensor frame $O_B - \boldsymbol{X}_S\boldsymbol{Y}_S\boldsymbol{Z}_S$, where $\boldsymbol{X}_S$ is opposite to the sensor spin axis, $\boldsymbol{Z}_S$ is orthogonal to the spin axis, the fixed sensor reference is in the plane $O_B - \boldsymbol{Z}_S\boldsymbol{X}_S$, and $\boldsymbol{Y}_S$ completes the right-handed triad; and 4) the auxiliary measurement frame $O_B - \boldsymbol{X}_A\boldsymbol{Y}_A\boldsymbol{Z}_A$, which is defined by the sensor spin axis and the satellite position vector $\boldsymbol{r}$ pointing from O_I to O_B as $\boldsymbol{X}_A = \boldsymbol{X}_S$, $\boldsymbol{Y}_A = (\boldsymbol{X}_A \times \boldsymbol{r}^0)/|\boldsymbol{X}_A \times \boldsymbol{r}^0|$, and $\boldsymbol{Z}_A = \boldsymbol{X}_A \times \boldsymbol{Y}_A$, where $\boldsymbol{r}^0$ is the unit vector of $\boldsymbol{r}$. Figure 1 illustrates the geometry of the reference frames.

Received Aug. 8, 1997; revision received July 6, 1998; accepted for publication Sept. 2, 1998.

*Visiting Scholar, Gravity Probe B, W. W. Hansen Experimental Physics Laboratory.